Germ-line mutations in *WDR77* predispose to familial papillary thyroid cancer

Yanyang Zhao[a,b], Tian Yu[a,b,c], Jie Sun[d], Feiliang Wang[e], Chaoze Cheng[f], Shurong He[g], Lan Chen[g], Donghui Xie[c], Liping Fu[c], Xuhuizi Guan[a,b,c], An Yan[a,b], Yao Li[c], Gang Miao[c,1], and Xiaoquan Zhu[a,b,1]

[a]Key Laboratory of Geriatrics, Beijing Hospital, National Center of Gerontology, National Health Commission, Beijing 100730, China; [b]Institute of Geriatric Medicine, Chinese Academy of Medical Sciences, Beijing 100730, China; [c]Department of General Surgery, Beijing Hospital, National Health Commission, Beijing 100730, China; [d]Graduate School of Peking Union Medical College, Chinese Academy of Medical Sciences, Beijing 100730, China; [e]Department of Ultrasonography, Beijing Hospital, National Health Commission, Beijing 100730, China; [f]Research & Development, Mingma Technologies Co., Ltd., Shanghai 200131, China; and [g]Department of Pathology, Beijing Hospital, National Health Commission, Beijing 100730, China

Edited by Mary-Claire King, University of Washington, Seattle, WA, and approved June 17, 2021 (received for review January 6, 2021)

The inheritance of predisposition to nonsyndromic familial nonmedullary thyroid cancer (FNMTC) remains unclear. Here, we report six individuals with papillary thyroid cancer (PTC) in two unrelated nonsyndromic FNMTC families. Whole-exome sequencing revealed two germ-line loss-of-function variants occurring within a 28-bp fragment of *WDR77*, which encodes a core member of a transmethylase complex formed with the protein arginine methyltransferase PRMT5 that is responsible for histone H4 arginine 3 dimethylation (H4R3me2) in frogs and mammals. To date, the association of *WDR77* with susceptibility to cancer in humans is unknown. A very rare heterozygous missense mutation (R198H) in *WDR77* exon 6 was identified in one family of three affected siblings. A heterozygous splice-site mutation (c.619+1G > C) at the 5′ end of intron 6 is present in three affected members from another family. The R198H variant impairs the interaction of WDR77 with PRMT5, and the splice-site mutation causes exon 6 skipping and results in a marked decrease in mutant messenger RNA, accompanied by obviously reduced H4R3me2 levels in mutation carriers. Knockdown of *WDR77* results in increased growth of thyroid cancer cells. Whole-transcriptome analysis of *WDR77* mutant patient-derived thyroid tissue showed changes in pathways enriched in the processes of cell cycle promotion and apoptosis inhibition. In summary, we report *WDR77* mutations predisposing patients to nonsyndromic familial PTC and link germ-line *WDR77* variants to human malignant disease.

familial papillary thyroid cancer | predisposition | germ-line mutations | *WDR77*

The incidence of thyroid cancer has increased rapidly (1, 2). Approximately 95% of all cases of thyroid cancer are nonmedullary thyroid cancer (NMTC) of follicular cell origin. Several large population-based studies have shown a high familial risk of NMTC, which strongly suggests that hereditary factors are involved in the disease (3–7). However, the genes involved in predisposition to NMTC are poorly understood. Familial NMTC (FNMTC) accounts for up to 15% of all cases of thyroid tumors and includes syndromic and nonsyndromic tumors (8, 9). The genetic events in syndromic FNMTC are known (8, 9), while the genetic basis of nonsyndromic FNMTC remains unclear, although several chromosomal loci (1p13.2-1q22, 2q21, 14q32, 19p13.2, and 8p23.1-p22) (10–14) and low-penetrance mutations in *SRGAP1*, *NKX2.1*, *FOXE1*, *HABP2*, and *CHEK2* have been identified to confer susceptibility to nonsyndromic FNMTC (8, 13, 15–17).

WDR77 (also known as *MEP50*) is located on human chromosome 1p13.2. WDR77 is a core component of a transmethylase complex with the protein arginine methyltransferase PRMT5. WDR77 contains seven WD40-repeat (WDR) domains, the majority of which bind to the surface of PRMT5 and form a heterooctameric PRMT5 4:WDR77 4 complex (18). It recruits the substrate to PRMT5 and activates PRMT5 to methylate a specific arginine to dimethylarginines in target proteins such as histone H4 (18, 19).

Here, we reported six affected individuals with thyroid cancer from two unrelated Chinese families (F3 and F4) (Fig. 1*A* and *Materials and Methods*). Tumor tissue samples from four affected family members were analyzed with hematoxylin–eosin staining, which provided pathological confirmation of papillary thyroid cancer (PTC) (Fig. 1*B*). We subsequently performed whole-exome sequencing (WES) in the proband and in patients from the two families in order to identify new predisposing genes of thyroid cancer and expand our current understanding of the genetic basis of the disease.

Results

In this study, WES data were generated using peripheral-blood DNA from the affected individuals of two families with PTC (*SI Appendix, Supplementary Materials and Methods*). Utilizing filtering criteria (*SI Appendix*, Table S1), we identified two heterozygous variants, a missense variant, and a splice-site mutation located in exon 6 and at the boundary between exon 6 and intron 6 of *WDR77*, respectively, both of which occur within a DNA fragment of 28 bp (Fig. 2*A*). The two variants were then validated in the corresponding affected family members by Sanger sequencing, indicating an autosomal dominant inheritance pattern of PTC associated with mutations in *WDR77* (Fig. 1*A* and *SI Appendix*, Table S2).

The missense variant that was identified in family 3 results in a G-to-A substitution in *WDR77* (Chr.1:111,986,515, rs768526334, c.593G > A), which was present in the proband (F3_Patient III.7) and two other affected family members (F3_Patients III.2

Significance

Familial nonmedullary thyroid cancer (FNMTC) accounts for up to 15% of all thyroid tumors. Here, we report two germ-line loss-of-function variants in *WDR77* in two unrelated families with NMTC. *WDR77* is expressed in diverse human tissues. It forms a complex with the protein arginine methyltransferase PRMT5 and mediates H4R3me2 in frogs and mammals. Functional analyses show that *WDR77* variants impair formation of the complex of WDR77–PRMT5, resulting in reduced H4R3me2 in patients. Knockdown of *WDR77* results in increased growth of thyroid cancer cells. Taken together, our findings reveal a predisposing gene of FNMTC and expand the variant profile predisposing to FNMTC. Additionally, this report presents germ-line variants in *WDR77* associated with human disease.

Author contributions: Y.Z., G.M., and X.Z. designed research; Y.Z., T.Y., J.S., F.W., and X.Z. performed research; D.X., L.F., X.G., A.Y., and Y.L. contributed new reagents/analytic tools; Y.Z., C.C., S.H., L.C., G.M., and X.Z. analyzed data; and Y.Z., G.M., and X.Z. wrote the paper.

The authors declare no competing interest.

This article is a PNAS Direct Submission.

Published under the PNAS license.

[1]To whom correspondence may be addressed. Email: zhuxiaoquan3692@bjhmoh.cn or miaogang2633@bjhmoh.cn.

This article contains supporting information online at https://www.pnas.org/lookup/suppl/doi:10.1073/pnas.2026327118/-/DCSupplemental.

Published July 29, 2021.

Downloaded at Palestinian Territory, occupied on November 27, 2021

www.manaraa.com

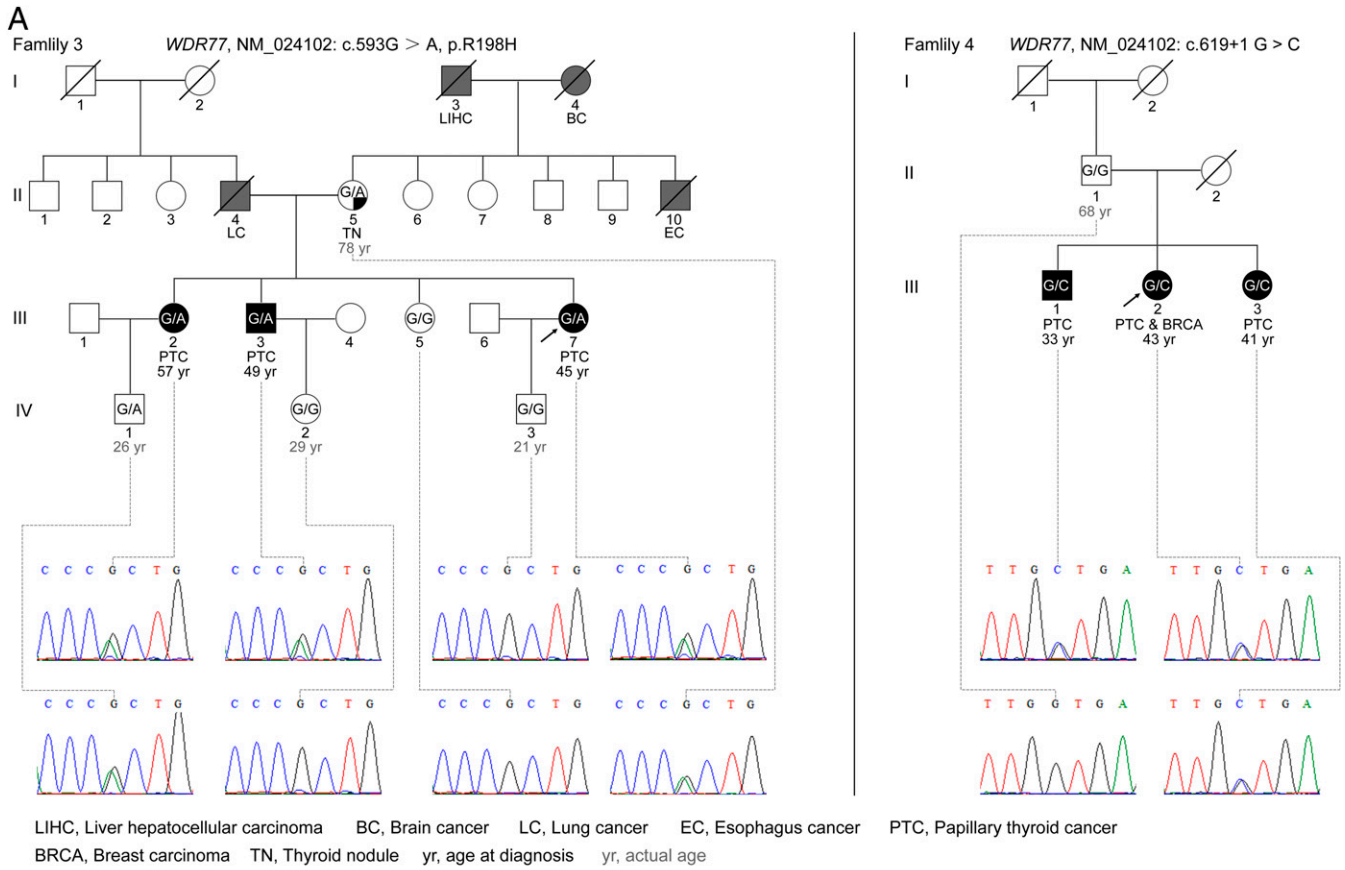

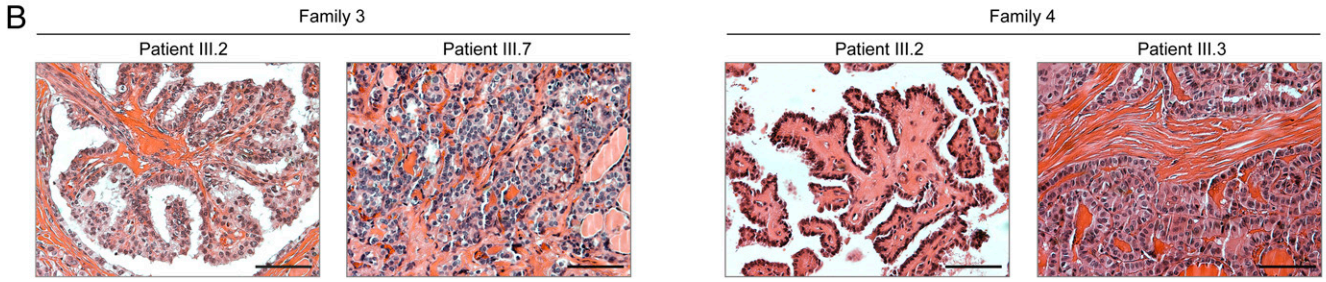

Fig. 1. Identification of *WDR77* mutations in two affected families. (*A*) Pedigree of two affected families (family 3 and family 4) and DNA sequence electropherograms showing mutations with the disease phenotype. Arrows indicate probands. No clinical information regarding the thyroid of F4_II.2 is available. Thyroid cancer in the affected family members with the splice-site mutation in family 4 occurred earlier (mean diagnosis age of 39 y) than in those with the R198H variant in family 3 (mean diagnosis age of 50.3 y), although this difference did not reach statistical significance; $P = 0.07$ by Student's t test. (*B*) Hematoxylin and eosin staining performed on tumor sections from F3_Patient III.2, F3_Patient III.7, F4_Patient III.2, and F4_Patient III.3. (Scale bars, 100 μm.)

and III.3) but was not in an unaffected sibling (F3_III.5) (Fig. 1*A*). The variant was also detected in the proband's 78-y-old mother (F3_II.5), who was found to have small thyroid nodules (4 to 5 mm) on imaging. Additionally, the variant was absent in 2,827 high-coverage exome sequences in a cancer-free in-house Chinese cohort (*SI Appendix, Supplementary Materials and Methods*), absent in 62,784 high-coverage genome sequences in TOPMed (Trans-Omics for Precision Medicine) (20) and in 141,431 low-coverage Chinese genome sequences (Chinese Millionome Database, CMDB) (21), and was only detected in 2 out of 125,722 persons in gnomAD (Genome Aggregation Database) version 2.1.1 (22). The G-to-A substitution converted an arginine to a histidine at position 198 of WDR77 (NM_024102, c.593G > A, p.R198H). The R198 residue is located in the fourth WDR domain and is well conserved in WDR77. Moreover, high conservation of the residue was also observed in RBBP4 and RBBP7, two of which are chromatin remodeling factors involved in chromatin assembly and cell proliferation by directly binding to the RB1 protein (23, 24) (Fig. 2*A*). The R198H variant was consistently predicted to be a disruptive mutation by SIFT (25), Polyphen2 (26), CADD (27), MutationAssessor (28) and fathmm (29) (Table 1).

To explore whether the *WDR77* R198H mutation was likely to interfere with protein function, we first examined the expression of the mutated *WDR77* transcript in the normal thyroid tissue and the matched tumor from the mutation carrier (F3_Patient III.2) by RT-PCR. Sequencing of the resulting RT-PCR products showed comparable expression abundance between wild-type and mutant alleles in thyroid tissues from the affected family member (*SI Appendix*, Fig. S1*A*). Similarly, no notable change in WDR77 protein level was detected between the tumor and the

Downloaded at Palestinian Territory, occupied on November 27, 2021
www.manaraa.com

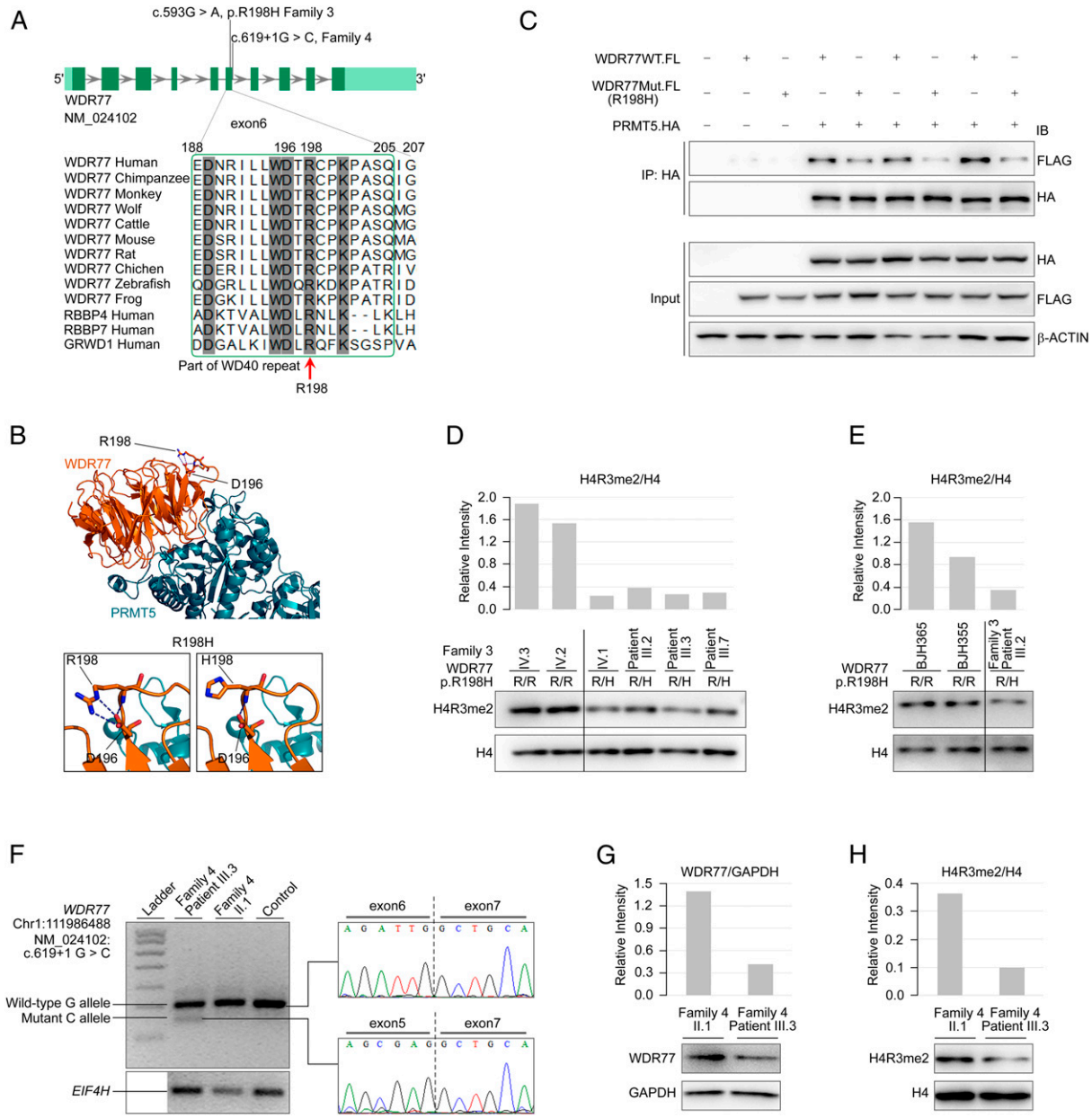

Fig. 2. The effect of *WDR77* mutations on histone H4R3 methylation. (*A*) Molecular genetic findings in patients with *WDR77* variants from these two families. Schematic of the exon–intron structure of *WDR77* showing the positions of one missense (c.593G > A, p.R198H) and one splice-site variant (c.619+1G > C). Conservation of the WD40 repeat (green rectangle indicated by a red arrow) and R198 across species are illustrated. RBBP4, RB Binding Protein 4. RBBP7, RB Binding Protein 7. GRWD1, Glutamate Rich WD Repeat Containing 1. (*B*, *Upper Panel*) The model of the complex of WDR77 (orange) and PRMT5 (cyan) (Protein Data Bank, 4gqb). (*Lower Panel*) Substitution of arginine to histidine at position 198 is predicted to cause loss of the hydrogen bond network. The hydrogen bond between Asp196 and Arg198 is highlighted. (*C*) The R198H mutation disrupts the interaction between WDR77 and PRMT5. 293T cells were transiently transfected with vectors expressing FLAG-tagged wild-type (lane 2) or R198H (lane 3) WDR77 protein alone or with HA-PRMT5 (lane 4 through lane 9). Immunoprecipitation was performed using an HA antibody, and immunoblotting was performed with anti-FLAG or anti-HA antibodies. (*D*) Immunoblotting shows the expression of histone H4 methylation in six samples taken from each F3 family member–derived peripheral WBCs (two unaffected family members without R198H mutation, F3_IV.2 and F3_IV.3; one unaffected member with R198H mutation, F3_IV.1; three affected members, F3_Patient III.2, III.3, and III.7). Total histone H4 served as loading control. Quantification of immunoblotting of H4R3me2 in F3 family members was performed. H4R3me2 intensity values were normalized against the levels of total histone H4. Experiments were repeated three times with similar results (see *SI Appendix*, Fig. S7*A* for details). (*E*) Immunoblotting shows the expression of histone H4 methylation in the normal thyroid tissues from the affected family member (F3_Patient III.2) and sporadic PTC patients without the mutation (BJH355 and BJH365). Total histone H4 served as loading control. Quantification of immunoblotting of H4R3me2 in the index patients was performed. H4R3me2 intensity values were normalized against the levels of total histone H4. Experiments were repeated three times with similar results (see *SI Appendix*, Fig. S7*C* for details). (*F*) PCR analysis shows the expression of *WDR77* mRNAs with the c.619+1G > C variant and wild-type *WDR77* mRNAs in F4 family member–derived peripheral WBCs (F4_Patient III.3 and an unaffected family member, F4_II.1). Control, *WDR77* mRNA expression levels in peripheral WBCs obtained from a sporadic case without the mutation. The *EIF4H* mRNA bands were indicated as a loading control. Marker, DNA marker. Sequence chromatograms of Sanger sequencing of *WDR77* mRNAs from F4_Patient III.3. (*G* and *H*) Immunoblotting shows the expression of WDR77 protein (*G*) and H4R3me2 (*H*) in F4 family member–derived peripheral WBCs (F4_Patients III.3 and F4_II.1). GAPDH and total histone H4 served as loading controls. Experiments were repeated three times with similar results (see *SI Appendix*, Fig. S7 *D* and *E* for details).

GENETICS

Downloaded at Palestinian Territory, occupied on November 27, 2021

www.manaraa.com

Table 1. Genetic and clinical characteristics of the individuals with *WDR77* mutations identified in this study

Patient number	F3_Patient III.2	F3_Patient III.3	F3_Patient III.7	F4_Patient III.1	F4_Patient III.2*	F4_Patient III.3
Sex	Female	Male	Female	Male	Female	Female
Base change	c.593G > A	c.593G > A	c.593G > A	c.619+1G > C	c.619+1G > C	c.619+1G > C
Amino acid change	p.R198H	p.R198H	p.R198H	—	—	—
Position	Exon 6	Exon 6	Exon 6	Donor splice site of intron6	Donor splice site of intron6	Donor splice site of intron6
MAF in Novo in-house cohort (n = 2,827)	Absence	Absence	Absence	Absence	Absence	Absence
MAF in CMDB (n = 141,431)	Absence	Absence	Absence	Absence	Absence	Absence
MAF in TOPMed (n = 62,789)	Absence	Absence	Absence	Absence	Absence	Absence
MAF in gnomAD (n =125,722)	0. 0008%	0. 0008%	0. 0008%	Absence	Absence	Absence
SIFT	Deleterious	Deleterious	Deleterious	—	—	—
Polyphen2	Probably damaging	Probably damaging	Probably damaging	—	—	—
MutationAssessor	Deleterious	Deleterious	Deleterious	Deleterious	Deleterious	Deleterious
CADD	35	35	35	26.1	26.1	26.1
fathmm	Pathogenic (0.979)	Pathogenic (0.979)	Pathogenic (0.979)	Pathogenic (0.983)	Pathogenic (0.983)	Pathogenic (0.983)
GERP++	5.94	5.94	5.94	5.94	5.94	5.94
Age at diagnosis (year)	57	49	45	33	43	41
Histologic type of cancer	PTC	PTC	PTC	PTC	PTC	PTC
Stage of cancer (TNM)[†]	T1aN0M0	T1bN1aM0	T1aN1aM0	NA	T1aN0M0	T1bN0M0
Radioiodine ablation	No	No	No	No	No	No
Vital status	Alive	Alive	Alive	Alive	Alive	Alive
Germ-line mutations tested for *PTEN*[‡], *APC*[‡], *DICER1*[‡], *WRN*[‡], *PRKAR1A*[‡], *STK11*[‡], *SPGAP1*[§], *NKX2.1*[§], *FOXE1*[§], *HABP2*[§], *CHEK2*[§]	WT	WT	WT	WT	WT	WT
Somatic mutations tested for *WDR77* mutations	c.6G > A, p.R2 =	NA	c.129C > T, p.L43= ; c.427G > A, p.G143D	NA	Negative	Negative
WDR77 CNAs	No change	NA	No change	NA	No change	No change
BRAF^{V600E}	Negative	NA	Negative	NA	Positive	Positive
KRAS, *NRAS*, *HRAS*, *TERT* c. 124C > T and c. 146C > T	Negative	NA	Negative	NA	Negative	Negative

NA, not available; MAF, mutant allele frequency.

*F4_Patient III.2 was also diagnosed with invasive ductal carcinomas of the breast.

[†]Staging was evaluated on the tumor-node-metastasis (TNM) classification of the American Joint Committee on Cancer and the Union for International Cancer Control, Eighth Edition.

[‡]Known syndromic FNMTC genes.

[§]Known predisposing genes to nonsyndromic FNMTC.

adjacent normal tissue in the mutation carriers (*SI Appendix*, Fig. S1 *B* and *C*). We also observed similar levels of WDR77 proteins between the mutation carriers and mutation noncarriers (*SI Appendix*, Fig. S2*A*). Since the R198 residue is very close to the nuclear localization sequence (144 to 197 residues) of WDR77 (30), we subsequently tested the localization of WDR77 in HEK293T cells overexpressing the wild-type or the R198H variant. Little difference in the localization of WDR77 was observed between wild-type– and *WDR77*–mutant HEK293T cells (*SI Appendix*, Fig. S1*D*).

When we modeled the R198H variant on the structure of the WDR77 protein, we found that the substitution to histidine at the R198 residue disrupted the formation of three backbone hydrogen bonds of R198 with D196, which was predicted to affect the stability of the β-turn that encompasses these two residues (Fig. 2*B*). This suggested destabilizing impact on the WDR domain likely interfered with the binding of WDR77 to PRMT5. Next, we established HEK293T cells coexpressing HA-PRMT5 with Flag-tagged wild-type WDR77 or with the WDR77 R198H variant. We found that the interaction between the WDR77 R198H mutant and PRMT5 was markedly decreased compared to that of wild-type WDR77 and PRMT5, as determined by coimmunoprecipitation assays (Fig. 2*C*).

Furthermore, peripheral white blood cells (WBCs) that were derived from four family members harboring R198H showed less dimethylation at arginine 3 of histone H4 (H4R3me2) than WBCs from two family members with wild-type *WDR77* (Fig. 2*D*), while no difference in WDR77 protein abundance was detected in any of these six individuals (*SI Appendix*, Fig. S2*A*). Similarly, reduced histone H4 methylation was also seen in the normal thyroid tissue from the mutation carrier (F3_Patient III.2) compared to those of mutation noncarriers (Fig. 2*E* and *SI Appendix*, Fig. S2*B*). Together, these results indicated that the R198H mutation impaired the binding of WDR77 with PRMT5, leading to a decrease in histone H4 methylation.

On the other hand, the splice-site variant in *WDR77* identified in family 4 (Chr.1:111,986,488, NM_024102, c.619+1G > C) was present in the proband (F4_Patient III.2) and her two affected siblings (F4_Patients III.1 and III.3) but not in her unaffected father (F4_ II.1) (Fig. 1*A*). In addition, the variant was absent from all public DNA sequence databases including TOPMed, gnomAD, and CMDB. The proband's mother (F4_II.2) died from kidney failure at the age of 58. She had noncalcified pulmonary nodules, but no medical information related to her thyroid was available.

This heterozygous c.619+1G > C mutation destroys a canonical splice donor site in intron 6. The effect of the splice-site mutation was determined using RT-PCR followed by Sanger sequencing of

Downloaded at Palestinian Territory, occupied on November 27, 2021

www.manaraa.com

WBCs derived from the affected family member (F4_Patient III.3) and her unaffected father (F4_II.1) (Fig. 2*F*). The mutation caused exon 6 skipping, consequently leading to a frameshift starting with an alanine at amino acid 189 and creating a premature stop codon at position 43 of the new reading frame (*SI Appendix*, Fig. S3). The shorter transcript from the mutant allele was observed at very low levels (Fig. 2*F*), suggesting that the mutation triggers the nonsense-mediated messenger RNA (mRNA) decay (NMD) process. Consistently, WDR77 protein levels were evidently decreased in the mutation carrier (F4_Patient III.3) compared to the mutation noncarrier (F4_ II.1) (Fig. 2*G*). Similar to the functional consequence of the R198H variant in *WDR77*, the c.619+1G > C mutation led to a lower level of histone H4 methylation in the mutation carrier (F4_Patient III.3) than in the mutation noncarrier (F4_II.1) (Fig. 2*H*). Together, these data indicated that both the missense variant and the splice-site mutation led to the loss of function of *WDR77* in the affected family members.

To further evaluate the putative biological effect of loss of function of *WDR77*, we conducted the knockdown of *WDR77* in two human thyroid cancer cell lines (TPC-1 and FTC-133) and a human embryonic kidney cell line (HEK293 cells) using two different small interfering RNAs (siRNAs)—si*WDR77*#1 and si*WDR77*#2 (31). The three cell lines carry no *WDR77* protein-coding or splice-site mutation. We observed that each of the two siRNAs was able to effectively inhibit WDR77 protein expression in these cell lines (Fig. 3*A* and *SI Appendix*, Fig. S4*A*). Cell proliferation assays showed that siRNA-mediated *WDR77* knockdown significantly increased the growth of TPC-1, FTC-133, and HEK293 cells (Fig. 3*A* and *SI Appendix*, Fig. S4*A*), suggesting that a decrease in WDR77 expression resulted in an increase in the growth of thyroid cancer cells.

As both *WDR77* R198H and the inactivated splice-site mutation altered histone modification status, we conducted RNA sequencing on normal thyroid tissues from an affected individual (F3_Patient III.2) and three sporadic PTC patients without the mutations (*SI Appendix*, Fig. S4*B*) to analyze the associated gene expression changes. We observed that 147 genes showed more than twofold up-regulation and that 116 genes had more than twofold down-regulation in the mutation carrier compared to those of three mutation noncarriers (*SI Appendix*, Fig. S4*C*). Analysis of cancer hallmark-associated genes in the gene expression profiles showed

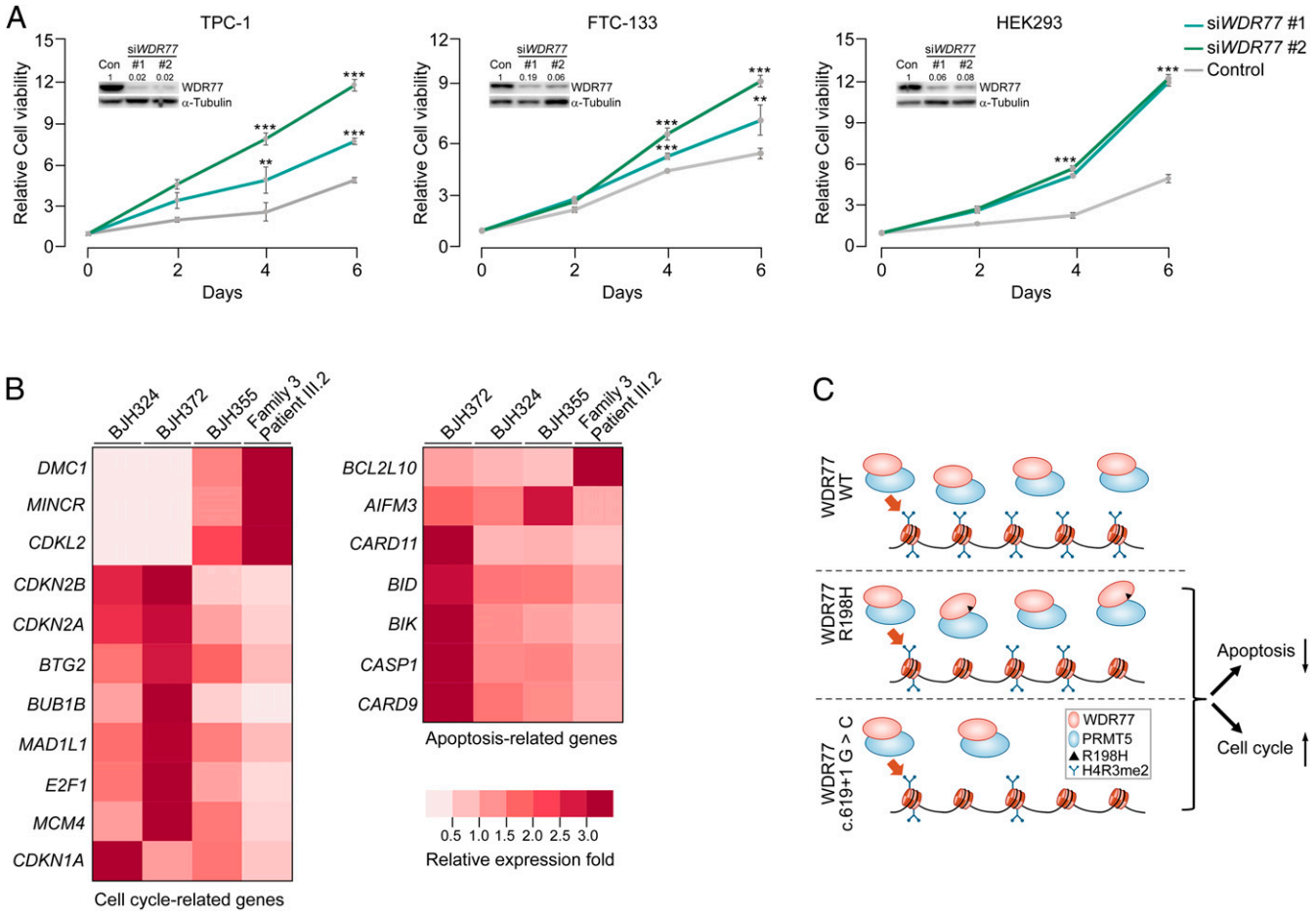

Fig. 3. Biological effect of loss of function of *WDR77*. (*A*) CellTiter-Glo assay was used to determine the growth of TPC-1, FTC-133, or HEK293 cells treated with the control siRNA and si*WDR77* (si*WDR77*#1, si*WDR77*#2), respectively, over a four-point time course. The data of representative experiments resulted from two independent experiments with four replicates per group. (*Inset*) Protein blot showing knockdown of WDR77 protein in the corresponding cell lines. Quantification relative to the levels in cells treated with the control siRNA of the total intensity of the WDR77 band relative to the alpha-tubulin band is shown above. Experiments were repeated with similar results (see *SI Appendix*, Fig. S4*A* for details). (*B*) Differentially expressed genes associated with the processes of the cell cycle and apoptosis by RNA sequencing of normal thyroid tissues from the affected family member (F3_Patient III.2) and sporadic PTC patients without the mutation (BJH324, BJH355, and BJH372). (*C*) Summary model of the biological effects of *WDR77* mutations in this study. (*Upper Panel*) The formation of the PRMT5:WDR77 complex is a key step for H4R3me2 modification. (*Middle* and *Lower Panels*) *WDR77* mutations diminish binding with PRMT5 or reduce the amount of the complex, resulting in a decrease in H4R3me2 levels, which might eventually regulate the expression of cancer hallmark–associated genes involved in promoting the cell cycle and inhibiting apoptosis. $^{**}P < 0.01$ and $^{***}P < 0.001$ by two-tailed Student's *t* test, mean ± SD; $n = 4$.

Downloaded at Palestinian Territory, occupied on November 27, 2021

www.manaraa.com

an increase in expression of genes for promoting cell cycle and suppressing cell apoptosis and a decrease in expression of genes for suppressing cell cycle and promoting cell apoptosis in the mutation carrier compared with controls (Fig. 3*B* and *SI Appendix*, Table S3).

Moreover, to examine the somatic mutation status of *WDR77* in thyroid tumors from the affected family members, we sequenced the whole coding regions and splicing sites of *WDR77* using genomic DNAs available from the formalin-fixed paraffin-embedded tumor specimens of four affected individuals (F3_Patient III.2, F3_Patient III.7, F4_Patient III.2, and F4_Patient III.3) (*SI Appendix*, Fig. S5). Three somatic single-nucleotide variants (two silent mutations and one missense mutation) were found in F3_Patient III.2 and F3_Patient III.7 (*SI Appendix*, Fig. S5*B* and Table 1). Furthermore, copy number analysis in the tumor samples showed no copy number alterations of *WDR77* compared with the matched blood DNA (Table 1). We also found no known somatic mutations in *KRAS*, *NRAS*, *HRAS*, or *TRET*, except *BRAF* in the tumor samples (Table 1).

Discussion

In summary, we reported that individuals with nonsyndromic FPTC harbored damaging germ-line mutations in *WDR77*, which resulted in impairment of the association of WDR77 with PRMT5. WDR77 in complex with PRMT5 is required for activation of PRMT5 to modify histone H4 (18, 19, 32). The disruption of the interaction between WDR77 and PRMT5 suppressed the methylation of histone H4 (33). Accordingly, we observed a reduction in the methylation of histone H4 in our affected family members. In engineered mouse models, mice fully lacking wdr77 die as early-stage embryos. *Wdr77*$^{+/-}$ heterozygous mice exhibited excessive epithelial cell proliferation that resulted in prostatic intraepithelial neoplasia and increased testis size (34, 35), suggesting that lacking one copy of the *WDR77* allele was sufficient to cause a propensity of proliferation of normal cells and that haploinsufficiency may be a mechanistic explanation for the lesion due to the low WDR77 protein level and, consequently, decreased methyltransferase activity of PRMT5. Likewise, a reduction of the activation of PRMT5 in human hematopoietic progenitor cells by using short hairpin RNA (shRNA) led to an increase in colony formation of the cells (36). Nevertheless, WDR77 plays roles in cell proliferation or differentiation depending on the cell context (31, 34–38). Our functional experiments showed that the reduced *WDR77* expression promoted human thyroid cancer cell proliferation. Our expression profile data of the normal thyroid tissues from mutation carriers and noncarriers indicated that differentially expressed genes were enriched in the processes of cell cycle promotion and apoptosis suppression, providing insight into the possible mechanism for the variants of *WDR77* predisposing to PTC (Fig. 3*C*). Moreover, we cannot rule out the possibility that the identified mutations could alter some currently unknown functions of *WDR77* that may contribute to predisposition.

Moreover, we analyzed two large population cohorts: the gnomAD (version 2.1.1 and version 3.1.1) datasets, which contain 125,748 exomes and 76,156 whole genomes from unrelated noncancer individuals and 132,345 deeply sequenced unrelated genomes from the TOPMed (freeze 8) dataset. We found 30 high-confidence predicted loss-of-function variants of *WDR77* in 55 gnomAD individuals and 41 TOPMed individual carriers, with a combined carrier frequency of 0.03% (*SI Appendix*, Fig. S6 and Dataset S1). Furthermore, we found 17 tumor samples with 14 somatic truncating variants, including 1 frameshift, 4 splicing, and 9 stop-gain mutations, in the Catalogue of Somatic Mutations in Cancer (39) and cBioPortal (40) databases (*SI Appendix*, Fig. S6*B* and Dataset S1). Notably, the search revealed a 29-y-old female thyroid cancer patient with a stop-gain mutation in *WDR77* (THYROID-CN-WZ040T, WDR p.C208*, c.624C > A), which could result in the loss of function of *WDR77*, similar to the consequence of the c.619+1G > C mutation identified in our study. Additionally, one *WDR77* somatic missense mutation combined with a deletion mutation in the gene was found in each of seven tumors (*SI Appendix*, Fig. S6*B* and Dataset S1). All these data further supported the association of heterozygous loss-of-function variants in *WDR77* with human disease.

Taken together, our findings identified two loss-of-function variants in *WDR77* predisposed to FNMPTC and established a link between germ-line *WDR77* mutations and human malignant disease.

Materials and Methods

Study Patients and Oversight. This study was approved by the Research Ethics Board of the Beijing Hospital, Ministry of Health. All participants provided written informed consent before participation. Family members in two families (F3_Patient III.2, F3_Patient III.3, F3_Patient III.7, F4_Patient III.2, and F4_Patient III.3) were admitted to our hospital during 2018 to 2020 due to thyroid neoplasms detected with ultrasound-guided fine-needle aspiration biopsy. The proband in family 3 (F3_Patient III.7), a 48-y-old woman, was the youngest of four children. Her mother (F3_II.5) is 78 y old and was found to have small thyroid nodules (4 to 5 mm) upon neck ultrasonography. F3_IV.1, a 26-y-old man, had undergone neck ultrasonography, and no thyroid nodule was found when undergoing evaluation in our study. The proband in family 4 (F4_Patient III.2), a 44-y-old woman, was diagnosed with breast cancer at age 36 and thyroid cancer at age 43. Her mother (F4_II.2) died from kidney failure at the age of 58. She had noncalcified pulmonary nodules, but no medical information related to her thyroid was available. All five patients (F3_Patient III.2, F3_Patient III.3, F3_Patient III.7, F4_Patient III.2, and F4_Patient III.3) were diagnosed with papillary thyroid carcinoma and received a thyroidectomy. None of the family members, except one member (F4_Patient III.2), had a history of other primary cancers. No other benign tumors were detected in the two families.

Genetic Testing and Function Analyses. We performed WES on Patient III.2 and Patient III.7 from family 3 and the Patient III.1 and Patient III.3 from family 4. Function analyses of the variants were performed. The detailed methods are available in *SI Appendix*.

Data Availability. All study data are included in the article and/or supporting information.

ACKNOWLEDGMENTS. This study was supported by the Beijing Hospital Clinical Research 121 Project Grant No. BJ-2020-169 (to G.M.); the Chinese Academy of Medical Sciences Innovation Fund for Medical Sciences Grant No. 2018-I2M-1-002 (to Y.Z.); the National Natural Science Foundation of China Grant No. 81872096 (to X.Z.), and Grant No. 81541152 (to Y.Z.); and the Beijing Natural Science Foundation Grant No. 7172194 (to G.M.). We thank all individuals who participated in the project and Bayi Xiao for work with the samples collected for PTC in Beijing Hospital.

1. L. Du *et al*., Incidence and mortality of thyroid cancer in China, 2008-2012. *Chin. J. Cancer Res.* **31**, 144–151 (2019).
2. H. Lim, S. S. Devesa, J. A. Sosa, D. Check, C. M. Kitahara, Trends in thyroid cancer incidence and mortality in the United States, 1974-2013. *JAMA* **317**, 1338–1348 (2017).
3. L. T. Amundadottir *et al*., Cancer as a complex phenotype: Pattern of cancer distribution within and beyond the nuclear family. *PLoS Med.* **1**, e65 (2004).
4. D. E. Goldgar, D. F. Easton, L. A. Cannon-Albright, M. H. Skolnick, Systematic population-based assessment of cancer risk in first-degree relatives of cancer probands. *J. Natl. Cancer Inst.* **86**, 1600–1608 (1994).
5. C. Dong, K. Hemminki, Modification of cancer risks in offspring by sibling and parental cancers from 2,112,616 nuclear families. *Int. J. Cancer* **92**, 144–150 (2001).
6. M. Fallah *et al*., Risk of thyroid cancer in first-degree relatives of patients with nonmedullary thyroid cancer by histology type and age at diagnosis: A joint study from five Nordic countries. *J. Med. Genet.* **50**, 373–382 (2013).
7. T. Pal *et al*., Increased risk for nonmedullary thyroid cancer in the first degree relatives of prevalent cases of nonmedullary thyroid cancer: A hospital-based study. *J. Clin. Endocrinol. Metab.* **86**, 5307–5312 (2001).
8. E. J. Son, V. Nosé, Familial follicular cell-derived thyroid carcinoma. *Front. Endocrinol. (Lausanne)* **3**, 61 (2012).
9. A. Khan, J. Smellie, C. Nutting, K. Harrington, K. Newbold, Familial nonmedullary thyroid cancer: A review of the genetics. *Thyroid* **20**, 795–801 (2010).
10. C. D. Malchoff *et al*., Papillary thyroid carcinoma associated with papillary renal neoplasia: Genetic linkage analysis of a distinct heritable tumor syndrome. *J. Clin. Endocrinol. Metab.* **85**, 1758–1764 (2000).

Downloaded at Palestinian Territory, occupied on November 27, 2021

www.manaraa.com

11. J. D. McKay *et al*., Localization of a susceptibility gene for familial nonmedullary thyroid carcinoma to chromosome 2q21. *Am. J. Hum. Genet.* **69**, 440–446 (2001).
12. G. R. Bignell *et al*., Familial nontoxic multinodular thyroid goiter locus maps to chromosome 14q but does not account for familial nonmedullary thyroid cancer. *Am. J. Hum. Genet.* **61**, 1123–1130 (1997).
13. S. Peiling Yang, J. Ngeow, Familial non-medullary thyroid cancer: Unraveling the genetic maze. *Endocr. Relat. Cancer* **23**, R577–R595 (2016).
14. B. M. Cavaco, P. F. Batista, L. G. Sobrinho, V. Leite, Mapping a new familial thyroid epithelial neoplasia susceptibility locus to chromosome 8p23.1-p22 by high-density single-nucleotide polymorphism genome-wide linkage analysis. *J. Clin. Endocrinol. Metab.* **93**, 4426–4430 (2008).
15. S. K. Gara *et al*., Germline *HABP2* mutation causing familial nonmedullary thyroid cancer. *N. Engl. J. Med.* **373**, 448–455 (2015).
16. Y. Zhao *et al*., A germline *CHEK2* mutation in a family with papillary thyroid cancer. *Thyroid* **30**, 924–930 (2020).
17. K. Hińcza, A. Kowalik, A. Kowalska, Current knowledge of germline genetic risk factors for the development of non-medullary thyroid cancer. *Genes (Basel)* **10**, 482 (2019).
18. S. Antonysamy *et al*., Crystal structure of the human PRMT5:MEP50 complex. *Proc. Natl. Acad. Sci. U.S.A.* **109**, 17960–17965 (2012).
19. E. S. Burgos *et al*., Histone H2A and H4 N-terminal tails are positioned by the MEP50 WD repeat protein for efficient methylation by the PRMT5 arginine methyltransferase. *J. Biol. Chem.* **290**, 9674–9689 (2015).
20. D. Taliun *et al*.; NHLBI Trans-Omics for Precision Medicine (TOPMed) Consortium, Sequencing of 53,831 diverse genomes from the NHLBI TOPMed Program. *Nature* **590**, 290–299 (2021).
21. S. Liu *et al*. Genomic analyses from non-invasive prenatal testing reveal genetic associations, patterns of viral infections, and Chinese population history. *Cell* **175**, 347–359.e14 (2018).
22. K. J. Karczewski *et al*.; Genome Aggregation Database Consortium, The mutational constraint spectrum quantified from variation in 141,456 humans. *Nature* **581**, 434–443 (2020).
23. Y. Zhang, R. Iratni, H. Erdjument-Bromage, P. Tempst, D. Reinberg, Histone deacetylases and SAP18, a novel polypeptide, are components of a human Sin3 complex. *Cell* **89**, 357–364 (1997).
24. Y. W. Qian, E. Y. Lee, Dual retinoblastoma-binding proteins with properties related to a negative regulator of ras in yeast. *J. Biol. Chem.* **270**, 25507–25513 (1995).
25. N. L. Sim *et al*., SIFT web server: Predicting effects of amino acid substitutions on proteins. *Nucleic Acids Res.* **40**, W452–W457 (2012).
26. I. A. Adzhubei *et al*., A method and server for predicting damaging missense mutations. *Nat. Methods* **7**, 248–249 (2010).
27. P. Rentzsch, D. Witten, G. M. Cooper, J. Shendure, M. Kircher, CADD: Predicting the deleteriousness of variants throughout the human genome. *Nucleic Acids Res.* **47** (D1), D886–D894 (2019).
28. B. Reva, Y. Antipin, C. Sander, Predicting the functional impact of protein mutations: Application to cancer genomics. *Nucleic Acids Res.* **39**, e118 (2011).
29. H. A. Shihab *et al*., Predicting the functional, molecular, and phenotypic consequences of amino acid substitutions using hidden Markov models. *Hum. Mutat.* **34**, 57–65 (2013).
30. Z. Gu, L. Zhou, S. Gao, Z. Wang, Nuclear transport signals control cellular localization and function of androgen receptor cofactor p44/WDR77. *PLoS One* **6**, e22395 (2011).
31. Y. Peng *et al*., Distinct nuclear and cytoplasmic functions of androgen receptor cofactor p44 and association with androgen-independent prostate cancer. *Proc. Natl. Acad. Sci. U.S.A.* **105**, 5236–5241 (2008).
32. M. C. Ho *et al*., Structure of the arginine methyltransferase PRMT5-MEP50 reveals a mechanism for substrate specificity. *PLoS One* **8**, e57008 (2013).
33. K. Saha, M. L. Fisher, G. Adhikary, D. Grun, R. L. Eckert, Sulforaphane suppresses PRMT5/MEP50 function in epidermal squamous cell carcinoma leading to reduced tumor formation. *Carcinogenesis* **38**, 827–836 (2017).
34. J. J. Liang *et al*., The expression and function of androgen receptor coactivator p44 and protein arginine methyltransferase 5 in the developing testis and testicular tumors. *J. Urol.* **177**, 1918–1922 (2007).
35. S. Gao, H. Wu, F. Wang, Z. Wang, Altered differentiation and proliferation of prostate epithelium in mice lacking the androgen receptor cofactor p44/WDR77. *Endocrinology* **151**, 3941–3953 (2010).
36. F. Liu *et al*., JAK2V617F-mediated phosphorylation of PRMT5 downregulates its methyltransferase activity and promotes myeloproliferation. *Cancer Cell* **19**, 283–294 (2011).
37. H. Qi *et al*., Sirtuin 7-mediated deacetylation of WD repeat domain 77 (WDR77) suppresses cancer cell growth by reducing WDR77/PRMT5 transmethylase complex activity. *J. Biol. Chem.* **293**, 17769–17779 (2018).
38. B. Vincent, H. Wu, S. Gao, Z. Wang, Loss of the androgen receptor cofactor p44/WDR77 induces astrogliosis. *Mol. Cell. Biol.* **32**, 3500–3512 (2012).
39. J. G. Tate *et al*., COSMIC: The catalogue of somatic mutations in cancer. *Nucleic Acids Res.* **47** (D1), D941–D947 (2019).
40. E. Cerami *et al*., The cBio cancer genomics portal: An open platform for exploring multidimensional cancer genomics data. *Cancer Discov.* **2**, 401–404 (2012).

Downloaded at Palestinian Territory, occupied on November 27, 2021

www.manaraa.com